Effect of oxygen challenge on MR imaging of tumor microenvironment

Zhongwei Zhang[1], Qing Yuan[1], Heling Zhou[1], and Ralph P Mason[1]
[1]*Department of Radiology, UT Southwestern Medical Center, Dallas, TX, United States*

Target Audience: Researchers interested in hypoxia and tumor microenvironment study.

Purpose: The microenvironment of solid tumors has been identified as a source of resistance to chemotherapy and radiotherapy, which was characterized as the diffusion and perfusion limitations within solid tumors and the resultant variable tissue oxygenation and acidification. Hypoxia modification using a high oxygen-content gas (i.e., 100% oxygen) has been shown to improve radiotherapy outcomes. Blood oxygen level-dependent (BOLD) and Tissue oxygen level-dependent (TOLD) MRI has been used to monitor the changes in blood and tissue oxygenation in response to oxygen inhalation in pre-clinical and clinical settings. However, BOLD and TOLD effects provide the macroscopic responses to oxygen challenge rather than the microstructure information itself. In normal brain, Federau et al[1] found that the IVIM perfusion parameters were reactive to hyperoxygenation-induced vasoconstriction and hypercapnia-induced vasodilatation. However, few studies have been performed to reveal the changes of tumor microenvironment such as diffusion and perfusion parameters in response to oxygen challenge. The purpose of this study was to evaluate the effect of oxygen challenge on tumor heterogeneity, diffusion and perfusion parameters at the microscopic level.

Methods: A well-characterized Dunning R3327-AT1 rat prostate cancer line was implanted subcutaneously in the thigh of male Copenhagen rats (~200 g, N=8). MRI was performed when tumors reached ~2 cm diameter. MRI used a horizontal bore 4.7-T system. Rats were imaged during breathing medical air (21% oxygen) followed by 100% oxygen. Physiological parameters, including respiratory, sO_2 and body temperature, were monitored during MRI scan. Diffusion-weighted images (DWI) with multiple b values (0, 25, 50, 100, 150, 200, 300, 500, 1000, 1500 s/mm^2) in three orthogonal directions were obtained using a multi-shot FSE-based Stejskal-Tanner DWI sequence (FSE-DWI). Axial images of tumor were acquired with slice thickness of 2 mm, in-plane resolution of 0.31×0.63 mm^2. TE/TR = 56/2000 ms, echo train length = 8. Data acquisition was repeated 3 times for baseline air and with 100% oxygen challenge, respectively. A standard IVIM two-compartment diffusion model was used[2], consisting of (1) a vascular compartment, occupying a fraction f of the tissue volume with a pseudo-diffusion coefficient Dp, and (2) a tissue compartment with diffusion coefficient Dt, i.e., $\frac{S_b}{S_0} = (1-f)e^{-b\cdot D_t} + fe^{-b\cdot D_p}$, where the S_b represents the signal intensity for each b value including the T_1 and T_2 relaxation effects, and S_0 is the initial signal intensity at b = 0 s/mm^2. A constrained two-step analysis (or "segmented" analysis) was performed to the signal decays to extract the 3 parameters f, Dp, and Dt. Apparent diffusion coefficient (ADC) was also calculated with the mono-exponential model: $\frac{S_b}{S_0} = e^{-b\cdot ADC}$. The stretched-exponential model[3], which yielded a measure of the moments of the intravoxel distribution of diffusion coefficients and heterogeneity in water diffusion, was also applied: $\frac{S_b}{S_0} = e^{-(b\cdot DDC)^{\alpha}}$, where DDC is the distributed diffusion coefficient, α is the heterogeneity index. Quantitative diffusion parameters were calculated on a voxel-by-voxel basis. A whole tumor region of interest (ROI) was drawn on diffusion images, and then copied to diffusion parametric maps. The mean and standard deviation were reported for each diffusion parametric map. Paired Student t test and Pearson correlation test were performed.

Results: Representative diffusion parametric maps are shown in Figure. Table shows the measured diffusion derived parameters with air and oxygen inhalation. Compared with air inhalation, a statistically significant increase of S_0 and a statistically significant decrease of blood volume fraction f were observed during oxygen challenge. No significance was found in ADC and Dt even though both values showed slight decrease during oxygen challenge. Both α and DDC showed significant changes with oxygen.

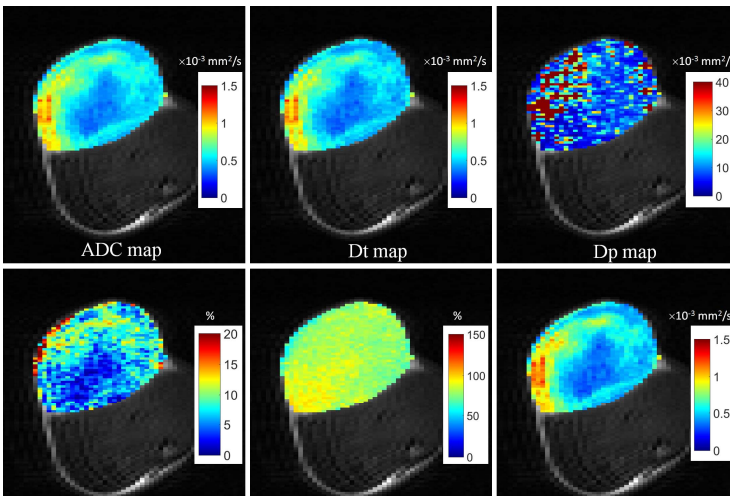

Representative diffusion parametric maps derived from IVIM model and stretched-exponential model fitting overlaid on T2W images

Discussion: The IVIM model demonstrated the significant decrease of blood volume fraction during oxygen challenge, which can be interpreted as a decreased perfusion in tumor microvasculature, and provides experimental evidence that active tumor neovasculature generates immature leaky blood vessels. No significant change of ADC and Dt during oxygen challenge demonstrated the expected independence of the diffusion coefficient in the nonvascular compartment. Instead, the stretched exponential model considers two types of intravoxel heterogeneity: heterogeneity in fluid viscosity and heterogeneity in diffusive restrictions. Our results indicated that α and DDC might provide a robust measure of tumor heterogeneity, which is sensitive to changes in fluid viscosity due to oxygen–induced perfusion decrease.

Conclusion: The current study demonstrated that IVIM diffusion MRI provided powerful insight into tumor perfusion. On the other hand, diffusion stretched-exponential model was sensitive to the changes of tumor heterogeneity, Combining these two models may serve as potential biomarker to evaluate tumor responses to oxygen.

Table: Effect of oxygen challenge on diffusion derived Parameters (* P < 0.05)

Rats (N = 8)	S_0 (b=0) (×10^3 a.u.)	ADC (×10^{-3} mm^2/s)	Dt(×10^{-3} mm^2/s)	Dp(×10^{-3} mm^2/s)	f (100%)	α (100%)	DDC (×10^{-3} mm^2/s)
Air	97.5 ±24.4	0.63±0.07	0.55±0.05	32.2±10.1	13.8±3.7	73.6±3.6	0.71±0.24
100% Oxygen	99.8 ±28.4	0.59±0.06	0.53±0.05	23.8±9.4	12.6±2.9	73.7±5.8	0.66±0.17
Pearson Correlation	0.96	0.64	0.67	-0.47	0.76	0.94	0.94
P Value	<0.001*	0.0876	0.068	0.2397	0.0275*	<0.001*	<0.001*

Acknowledgement: Supported in part by NIH R01 CA139043, P41 EB015908 & P30 CA142543

References:1. Federau C, et al. Radiology, 2012. 265(3): 874-881. 2. Le Bihan D, et al. Magn Reson Med, 1992. 27(1): 171-178. 3. Bennett et al. Magn Reson Med, 2003; 50:727-734.